THE FRACTAL DYNAMICS OF SATELLITE CAPTURE IN THE CIRCULAR RESTRICTED THREE-BODY PROBLEM

MARC A. MURISON[a)]
Department of Astronomy, University of Wisconsin–Madison, 475 North Charter Street, Madison, Wisconsin 53706
Received 19 June 1989; revised 1 September 1989

ABSTRACT

The structures of periodic orbit families in the circular restricted three-body problem are fractal-like. Successive magnifications of selected regions of the C–x_0 plane reveal that the families of periodic orbits are exceedingly complex and in some ways self-similar. Thus, satellite capture can be thought of as a competition between two primary masses for possession of the third particle, the boundary regions of the struggle being fractal. In addition, it is shown that an important mechanism of satellite capture involves the particle coming in (being captured) on a trajectory near the stable manifold of a hyperbolic fixed point near the inner Lagrangian point. The stable and unstable manifolds intersect transversally, resulting in chaotic motions and subsequent escape. Thus, gravitational capture is intimately associated with chaotic motion.

I. INTRODUCTION

The restricted three-body problem (RTBP) has been around a very long time (Euler 1772) and extensively studied by many (Szebehely 1967 and references therein). Orbit trajectories are usually quite complicated, so a simplified starting point for study has traditionally been periodic orbits. The importance of periodic orbits in understanding motions in the RTBP is emphasized by Poincaré's conjecture that, given a particular solution, one can find a periodic solution such that the difference between the two is negligible for arbitrary lengths of time. Thus, periodic orbits are of fundamental importance.

Much effort has been made towards calculating families of periodic orbits and determining their stability and their structures on the initial conditions space (see, e.g., Hénon 1965a,b, 1969c; Szebehely 1967). A family of periodic orbits can be represented by a curve (often called the characteristic curve) on the initial position–initial velocity plane. The usual approach is to substitute the Jacobi constant for initial velocity. This is done for several families, and relationships are explored, etc. In this paper a new viewpoint is offered regarding periodic orbit families in the restricted three-body problem.

As part of a project concerning satellite capture (Murison 1988, 1989b), the circular restricted three-body equations of motion were numerically integrated in a search for long, temporary capture orbits. The goal was to find the types of orbits around the more massive primary that are likely to be captured by the less massive primary for extended periods of time—i.e., to study the capture process. Results are presented elsewhere (Murison 1988, 1989b). Here we point out a curious phenomenon noticed in the course of this project—namely, that the structures corresponding to families of periodic orbits—that is, the characteristic curves—are fractal-like. We also partially investigate the phase space using the surface of section technique, finding that the fractal-like structures in the C–x_0 plane are related to the incredibly complex hierarchy of hyperbolic and elliptic fixed points; their associated "islands" of stability; and the migration, bifurcation, and eventual breakup into chaos of these islands.

In the next section, the method of calculation and the calculations themselves are described. In Sec. III, the fractal-like structures are presented. Section IV contains the surface of section analysis. The results are summarized in Sec. V.

II. DESCRIPTION OF CALCULATIONS

Even the plane circular RTBP has an initial parameter space of four dimensions to explore. This is much too complicated for initial numerical investigations. Thus, restrict the initial position to lie on the line joining the two primaries. Furthermore, let the initial velocity vector be at right angles to this line. Then the initial conditions space is two-dimensional: x_0, the initial position, and v_0, the initial velocity. Following Huang and Innanen (1983) and Hénon (1969c), we find it convenient to substitute the Jacobi constant C for the initial velocity, via the relation

$$v^2 = 2\Omega - C, \tag{1}$$

where

$$\Omega = \frac{1}{2}(x^2 + y^2) + \frac{1-\mu}{r_1} + \frac{\mu}{r_2},$$

$\mu = m_2/(m_1 + m_2)$, and r_1 and r_2 are the distances from m_1 and m_2. The units are such that the distance between the primaries is one, and the period of the primaries' orbit is 2π. The motion is viewed from the usual rotating reference frame, where m_1 and m_2 are fixed on the x axis at $x_1 = -\mu$ and $x_2 = 1 - \mu$.

The initial conditions as stated above produce a symmetric motion (Roy and Ovenden 1955). The symmetry is about both the x axis and the time axis. Thus, we need to calculate only half of the orbit. If the particle motion is begun in the sphere of influence of the smaller mass m_2, the subsequent capture time—the amount of time spent in motion around m_2—is then twice the amount of time elapsed before the particle *escapes* into motion around m_1. One can then plot the capture time, as a function of the initial conditions x_0 and C, as a contour or gray-scale plot. In practice, this means calculating individual orbits at the mesh points of a grid in the C–x_0 plane. During an integration, when the particle motion passes the inner Lagrangian point into mo-

[a)] Now at the Harvard–Smithsonian Center for Astrophysics.

 0004-6256/89/062346-14$00.90

tion around m_1, that orbit is terminated, the capture time recorded, and the next orbit started.

The numerical method used here for calculating orbits is that of Murison (1989a). Briefly, a Bulirsch–Stoer extrapolation method (Press *et al.* 1986) was combined with both two-body regularization (Stiefel and Scheifele 1970; Bettis and Szebehely 1971) and a manifold correction algorithm due to Nacozy (1971). This combination generally results in rms errors in the Jacobi constant of less than roughly 10^{-15}. Thus, the orbits are extremely accurate.

Table I lists the ranges in x_0 and C covered by the calculations that resulted in Fig. 1 [Plates 82–85]. For these calculations, the orbits were begun in initially prograde motion around m_2. Listed are the maximum calculation time limit for each orbit in units of the primary period (T), and the ranges in the initial conditions C and x_0 covered. For convenience, x from here on is referenced from m_1, not the center of mass. The actual capture time is, by symmetry, double the values shown. For Fig. 1(a), the grid is 200×200 orbits, while for the others it is 150×150 orbits.

The mass ratio here is $\mu = 0.01$, chosen mainly for convenience in viewing details in the C–x_0 diagrams (Figs. 1). Features in these diagrams evolve as the mass ratio varies (Murison 1989b), but the fractal-like structures continue to exist. The gross features in the $\mu = 0.01$ diagram are easily seen to be the evolved features in diagrams of smaller or larger μ. The 0.01 diagram has more separation between the large island structure and the upper structures than diagrams of smaller μ, and is therefore easier to use as an example. As far as the aims of showing that fractal-like structures exist and illustrating their association with the phase space structure of the dynamical system are concerned, there is no advantage in going to a more solar system-like mass ratio. These results are meant as a specific illustration of a general phenomenon of circular restricted three-body dynamics, and the precise value of μ is in this sense irrelevant.

Each individual orbit ran until one of the following occurred:

(1) The particle escaped out of the bubble around m_2 defined by the zero–velocity surface. By symmetry, these are capture orbits. Figure 2 shows an example of a typical short-capture orbit (both halves of the symmetric half-orbit which was actually calculated are shown).

(2) The integration time limit was reached. For these orbits, we do not know the eventual result, based on these calculations. Later we will use surface of section techniques to obtain clues to the outcomes of these orbits.

TABLE I. Initial conditions of Figs. 1(a)–1(h).

Fig.	x_0		C		T_{max}
1a	0.85	0.9995	3.15	3.16764	50
b	0.93	0.95	3.153	3.158	10
c	0.941	0.948	3.154	3.1555	10
d	0.9415	0.9438	3.1540	3.1545	10
e	0.94243	0.94298	3.15405	3.15415	25
f	0.94285	0.94340	3.15435	3.15448	20
g	0.94	0.96	3.1633	3.1665	20
h	0.9435	0.952	3.1652	3.1661	25

The choice of ranges of initial conditions for Fig. 1(a) were made as follows. The limits in x_0 were determined by the positions of the inner Lagrangian point and of m_2: $x(L_1) < x_0 < 1.0$. The upper limit for C was set by the value at which the zero–velocity bubble around m_2 closes off access to m_1—that is, when the energy of the particle is not large enough that it can pass between m_2 and m_1. The lower limit to C is somewhat arbitrary, but was chosen such that the zero–velocity surface begins to move away from m_2. These lower-boundary orbits are in general short-lived, in the sense that escape soon occurs from the vicinity of m_2. For values of C less than this, the energy of the particle is usually large enough that the capture lifetime is so short the term loses meaning.

III. C–x_0 STRUCTURE IN THE RESTRICTED THREE-BODY PROBLEM

In this section, we will see evidence of self-similarity in the C–x_0 diagrams. This kind of structure is telling us that the periodic orbit families are fractal-like.

Mandelbrot first coined the term fractal (see Mandelbrot 1982). His definition was that the Hausdorff–Besicovitch dimension of a fractal object exceeds the topological dimension, which is always an integer. Popular examples are Koch curves and Cantor sets. One of the common characteristics of a fractal is self-similarity. Thus, a less restrictive definition is "a fractal is a shape made of parts similar to the whole in some way" (Mandelbrot 1986; also Feder 1988). It is this latter definition that we will keep in mind here.

a) A Magnification Sequence of Portions of the C–x_0 Plane

Figure 1(a) is a C–x_0 diagram for $\mu = 0.01$. The capture time is represented by the gray scale, ranging from the shortest, assigned black, to the longest, assigned white. The next figure, Fig. 1(b), is an enlargement of the lower boxed region of Fig. 1(a). Notice how the vague features of Fig. 1(a) pop into sudden and complicated clarity, with indications of even more unresolved structure. Figure 1(c) is a magnification of the small box of Fig. 1(b). We see that indeed there is much more structure.

It is here where we first notice self-similar features. As we go from the lower right-hand corner to the upper left-hand corner in Fig. 1(b), we encounter first a thick arm, followed by a large blank space, followed by a smaller arm, then another space, then another three arms separated by spaces. In the magnification of a section of the largest arm [Fig. 1(c)], we see a quite similar pattern. In the region just above the top of the box, near $(x_0, C) = (0.943, 3.1546)$, there is an "arm," followed by a space, then another arm, then a space, then two more arms before we lose further detail to lack of resolution. The proportions of the two patterns appear to be similar. It seems that there is a copy of the larger "arm" structure of Fig. 1(b) embedded in the largest arm itself.

Figure 1(d) is an enlargement of the box of Fig. 1(c). The arm structure is clarified a little more in the upper left. In the region around the upper left corner of the lower box, near $(x_0, C) = (0.9425, 3.154\,15)$, there is another copy of the arm structure all over again. This probably continues without end.

Notice now, in Fig. 1(d), the pitchfork pattern in the upper right-hand corner, enclosed by a box. This pattern is repeated in the magnification of the lower box of Fig. 1(d), as shown in Fig. 1(e) in the upper center. Near the bottom of

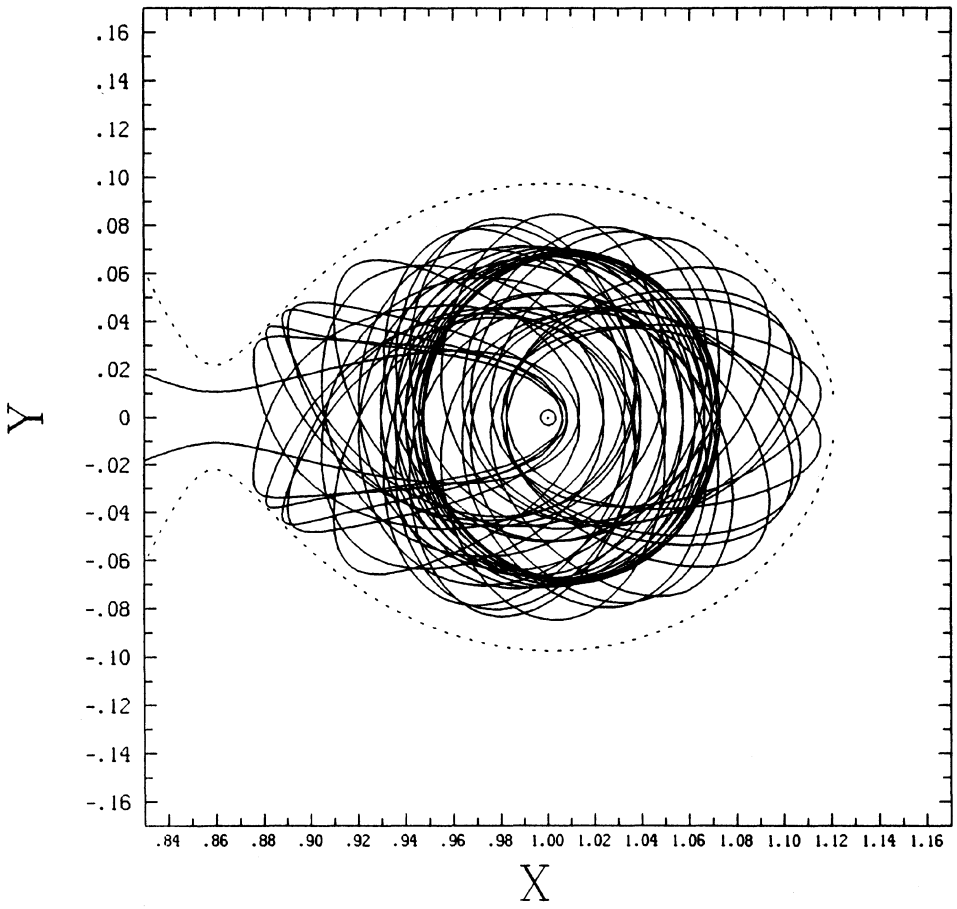

FIG. 2. Example of a typical escape/capture orbit. The dotted line is the zero-velocity curve.

Fig. 1(e) we see yet another copy of this same pattern, though poorly resolved. Figure 1(f) is the magnification of the upper box of Fig. 1(d).

Finally, Fig. 1(g) is a blow-up of the upper box of Fig. 1(a). Figure 1(h) is a magnification of the box of Fig. 1(g). The lower middle arc structure of Fig. 1(h) is similar to the middle arc structure of Fig. 1(g). The uppermost, thickest, middle arc of Fig. 1(g) appears to have a miniature copy of the whole structure embedded within itself. This also probably repeats *ad infinitum*.

These self-similar structures indicate that the periodic orbit structures in the C–x_0 plane are self-similar; that is, fractal. In hindsight, this may not be too surprising. The capture phenomenon can be viewed as a "competition" between m_1 and m_2 for the possession of the particle m. In very-short-capture regions of the C–x_0 plane, m_1 has the clear dominance; in the infinitely long-capture regions, m_2 is the uncontested winner. It is in the in-between regions that things get very interesting, and fractal structure appears. These are the "border" regions, the boundary between the influences of m_1 and m_2. Fractal structures tend to occur at the boundaries of attracting regions (see, e.g., McDonald *et al.* 1985; Peitgen and Richter 1986). Thus, *satellite capture is a boundary effect, and the boundary is fractal.*

b) The Periodic Orbit Connection

As discussed elsewhere (Murison 1988, 1989b), the many strands and loops apparent in Figs. 1 are associated with periodic orbit (p.o.) families. As we pick initial conditions closer and closer to a stable periodic orbit, the capture time increases until, past a certain point, the capture time becomes infinite (approximately the white regions in Figs. 1). If the p.o. is unstable, the capture time reaches some finite peak. Thus, a strand on the C–x_0 plane is tracing out a family or families of periodic orbits. A periodic orbit family lies under and is the cause of all of the loops and strands in the C–x_0 diagrams. Since the structures appear to be fractal, we conclude that the periodic orbit structure in the C–x_0 plane is fractal.

The large "island" feature of Fig. 1(a) results from the stable branch of a period 1 p.o. family. This family comes into existence through a bifurcation at the top of the island, in which stable and unstable families of periodic orbits suddenly and simultaneously appear. The unstable branch drops down to the left, and the stable branch drops down to the right. The orbit marked S1a in Figs. 1(a) and 1(b) (see also Fig. 5) is a member of the unstable branch, while the orbit marked S1b is a member of the stable branch.

The orbit sequences in Figs. 3–5 illustrate some of the p.o. families corresponding to a few of the more obvious strands in Fig. 1(a). The orbits in Figs. 3–5 are represented by the labeled dots in Figs. 1(a) and 1(b). In Fig. 3 we have the orbits labeled C; these are period 1,3,5, and 7 unstable orbits. Very close to them on the C–x_0 plane are the F orbits of Fig. 4. These are also period 1,3,5, and 7, and are unstable. Since these orbit families are unstable, even orbits precisely coinciding with one of the periodic orbits will escape after a finite

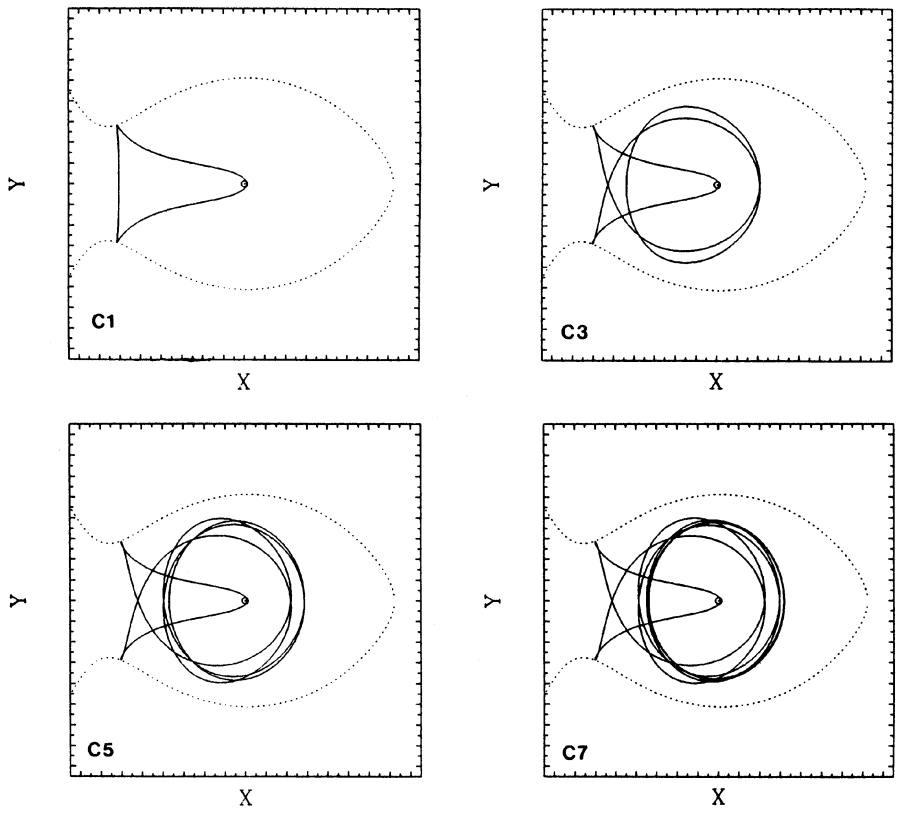

FIG. 3. Periodic orbits labeled C1, C3, C5, and C7 in Fig. 1(a).

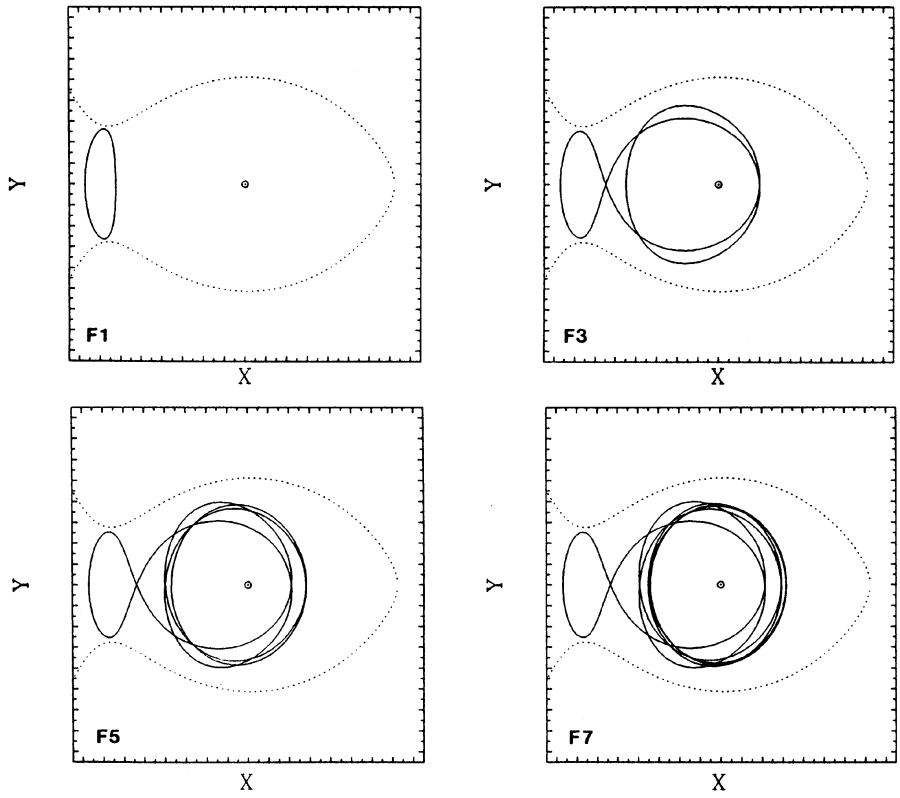

FIG. 4. Periodic orbits labeled F1, F3, F5, and F7 in Fig. 1(a).

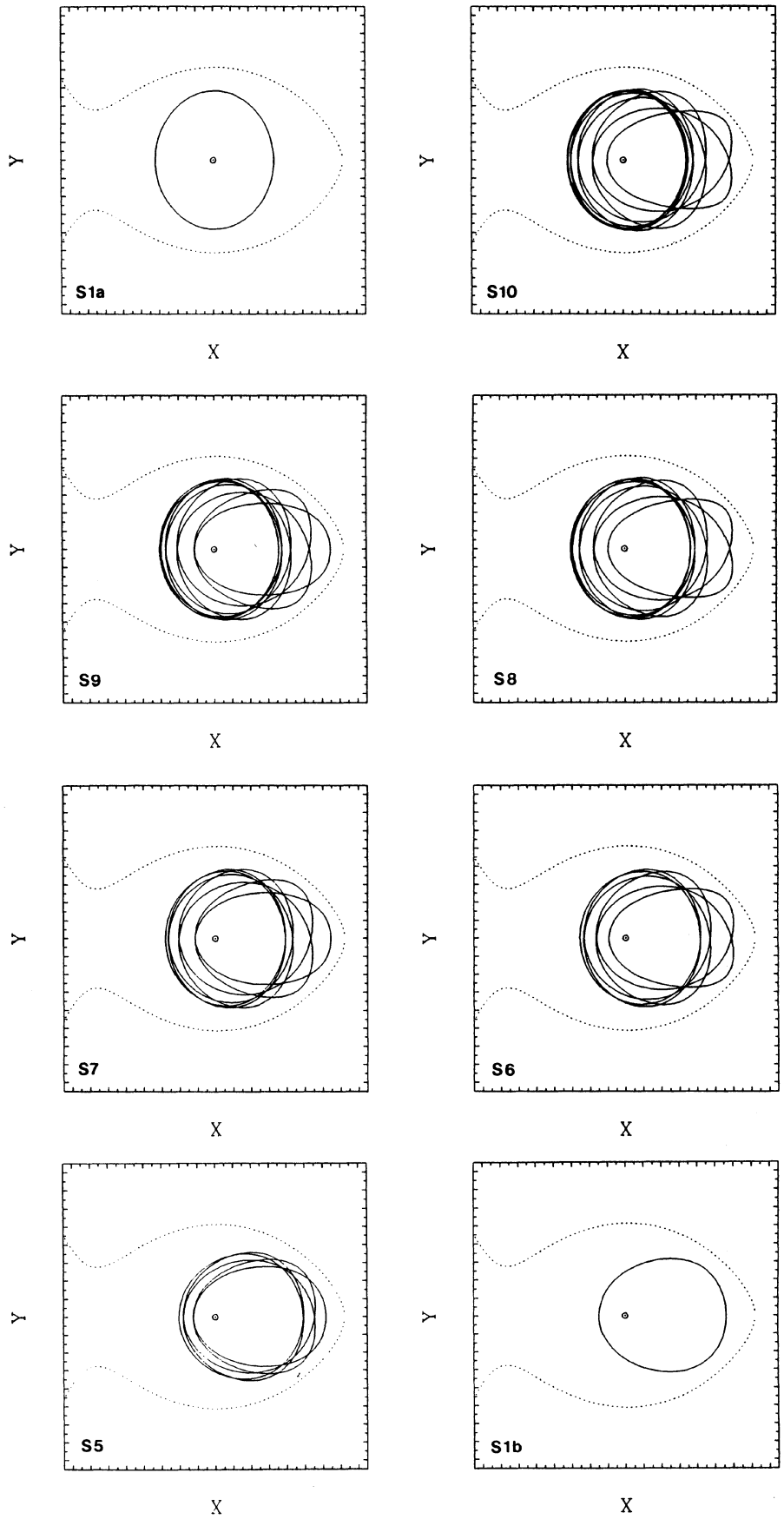

FIG. 5. Periodic orbits labeled S1a, S10, S9, S8, S7, S6, S5, and S1b in Figs. 1(a) and 1(b).

time. Figure 5 shows the S orbit sequence. Unlike the C and F orbits, for which n is odd, the S orbits can have n odd or even. But, again, except for S1b, the S orbits shown are unstable. Each of these families of unstable p.o. have their stable analogs tracing out a path in the white island region of Fig. 1(a). Buried in the island, and also in the stability region at the top of that figure, is a complex network of bifurcations of p.o. families. Some of these bifurcations have resulted in the family sequences illustrated here.

c) An Example of a Period-Doubling Bifurcation

Period-doubling bifurcations, among other kinds, occur in the restricted three-body problem. Figure 1(f) above looks suspiciously like just such an example. Periodic orbits were found at the locations of the labeled dots (G0–G3) in that plot.

The orbit labeled G0 is a period 11 orbit (that is, it loops around m_2 eleven times before closing). It is shown in Fig. 6(a) below. If the structure of Fig. 1(f) is a period-doubling bifurcation, then we would expect orbits G1 and G2 to be period 22. That is indeed the case. Orbit G1 is shown in Fig. 6(b). Close examination reveals a splitting of the trajectory.

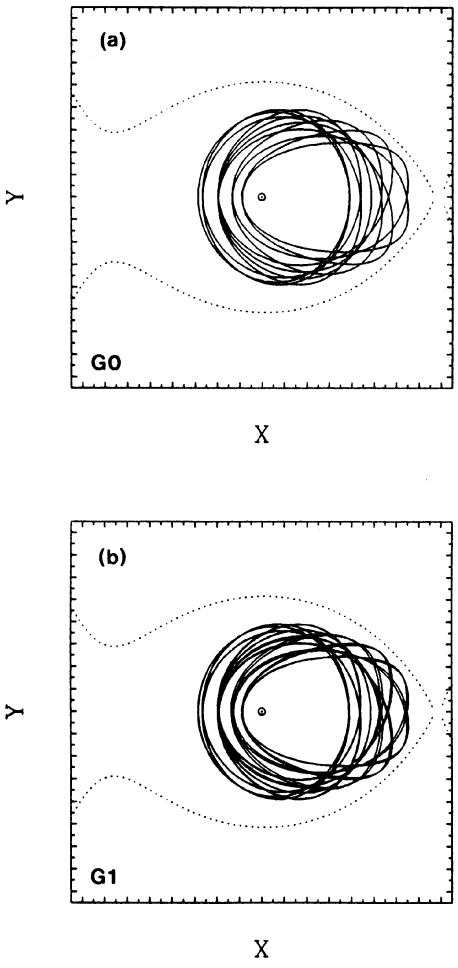

FIG. 6. (a) Period 11 orbit G0 of Fig. 1(f). (b) Period 22 orbit G1.

Finally, the orbit G3 is a member of the continuation of the period 11 family of orbit G0. The initial conditions and periods of motion are listed in Table II, along with those of the S, F, and C periodic orbits.

The other pitchfork structures mentioned above are also period-doubling bifurcations. The structure enclosed in the bottom box of Fig. 1(d) [also in the upper center of Fig. 1(e)] is a family of period 15 orbits bifurcating into sets of period 30 orbits. The squashed pitchfork at the bottom of Fig. 1(e) results from a period 19 family bifurcating into period 38.

IV. SURFACE OF SECTION ANALYSIS

One of the most useful tools available for investigating the phase space structure of a dynamical system is the surface of section (see, e.g., Jefferys 1974; Hénon 1983). The circular plane RTBP is a system of two degrees of freedom, with one integral (the Jacobi constant). Thus, the motion is confined to a three-dimensional hypersurface embedded in the four-dimensional phase space. A surface of section (sos) then is a two-dimensional cross section of the hypersurface. Here, similar to Hénon (1969a,b), we choose the surface $\{x,dx/d\theta \,|y = 0, dy/d\theta < 0\}$, where θ is the true anomaly of the orbit of the primaries (for the circular RTBP, θ is proportional to time t). Thus, every time a trajectory crosses the x axis in the rotating frame, and is moving in the negative y direction, a point is plotted on the $x,dx/d\theta$ plane.

If a particular trajectory happens to be in a region of phase space that is completely integrable, then it will lie on a two-dimensional subspace that is topologically a 2-torus. If the corresponding rotation number, $\nu = \omega_1/\omega_2$, defined as the ratio of the frequencies of motion along the "long" and

TABLE II. Periodic orbit parameters.

orbit	C	x_0	T
G0	3.15443	0.94319519	3.1686
G1	3.15441	0.94299626	6.3429
G2	3.15441	0.94329550	6.3429
G3	3.15440	0.94309241	3.1751
S1a	3.1555	0.9356555	0.2370
S10	3.1555	0.93742234	2.5622
S9	3.1555	0.9388144	2.3519
S8	3.1555	0.9403159	2.0907
S7	3.1555	0.9440606	1.8828
S6	3.1555	0.94835279	1.6298
S5	3.1555	0.95940005	1.4285
S1b	3.1555	0.97060297	0.2928
C1	3.1555	0.87836839	0.4614
C3	3.1555	0.91186970	0.9358
C5	3.1555	0.92635480	1.3928
C7	3.1555	0.93206996	1.8616
F1	3.1555	0.87500239	0.4396
F3	3.1555	0.91036892	0.9125
F5	3.1555	0.92573096	1.3669
F7	3.1555	0.93182711	1.8351

"short" directions of the torus, is irrational, then the intersections with the surface of section will trace out and fill a closed curve. The motion is quasiperiodic. If ν is rational, the motion is periodic, and the surface of section consists of a finite number of individual points. Suppose $\nu = m/n$, where m and n are integers. Then there are $k = m \times n$ points, and the corresponding orbit is period k.

A classic structure on the sos for a fully integrable Hamiltonian system is the saddle loop sketched in Fig. 7(a). Point P is a hyperbolic point, corresponding to an unstable period 1 p.o. Q is an elliptic point, corresponding to a stable period 1 p.o. The unstable invariant manifold of P, W^u, wraps around Q and joins smoothly the stable invariant manifold, W^s. If this structure is perturbed, rendering the system nonintegrable, then W^s and W^u can cross transversally, as illustrated in Fig. 7(b) (point R). This leads to the well-known homoclinic tangle, which implies a sensitive dependence on initial conditions, leading to chaotic dynamics (see, e.g., Guckenheimer and Holmes 1983; Hénon 1983; Helleman 1984; Wiggins 1988; Ruelle 1989). Poincaré (1892, 1893, 1899) first discovered the homoclinic tangle while studying the RTBP.

Figure 8(a) shows a surface of section for $C = 3.160\,36$. Several orbits were sampled along the horizontal line labeled A in Fig. 1(a). At this value of the Jacobi constant, the phase space structure is dominated by a saddle loop, with the unstable and stable fixed points near $x = 0.939$ and 0.959, respectively. At the resolution of the figure, the quasiperiodic trajectories encircling the elliptic fixed point appear to exist almost all the way to the hyperbolic fixed point. This indicates that in this region of phase space the system is nearly completely integrable.

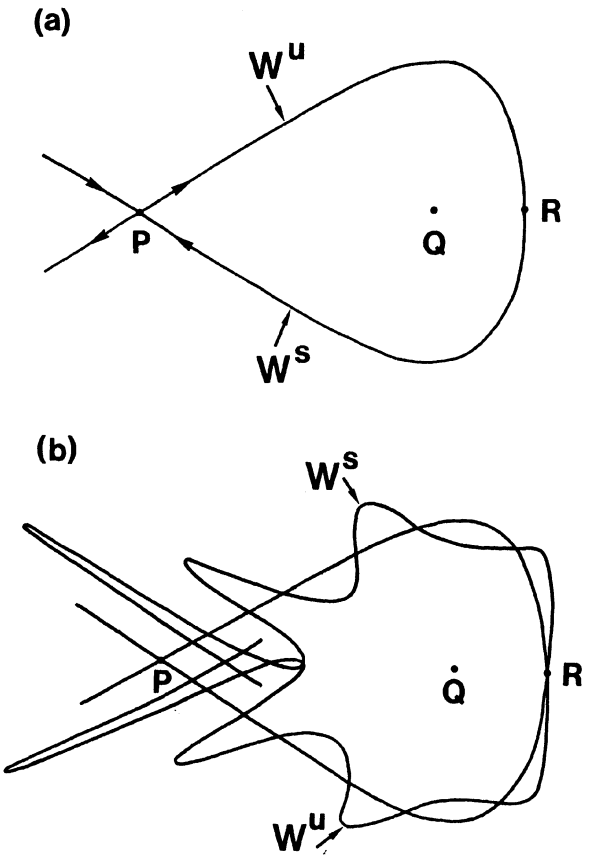

FIG. 7. (a) Unperturbed saddle loop structure on a surface of section. The stable and unstable invariant manifolds, W^s and W^u, join smoothly at point R. (b) A perturbed saddle loop. W^s and W^u cross transversally at R, giving rise to oscillations of the manifolds and a subsequent homoclinic tangle.

What happens if we decrease C? This corresponds to a higher "energy" of the massless particle, and a stronger perturbation by m_1. Figure 8(b) is an sos constructed from orbits sampled along the horizontal line labeled B in Fig. 1(a), at which the value of C is 3.157 24. We see that the elliptic point has given birth to a period 6 cycle, which manifests itself as the six elliptic islands. In fact, between $C = 3.160\,36$ and 3.157 24 several different n cycles and their associated islands have "flowed" out of the elliptic point and pushed their way outwards through the quasiperiodic region. Surrounding the quasiperiodic region of Fig. 8(b) are the islands associated with a period 7 family of orbits, which has been caught in the process of breaking up into the surrounding chaotic region. One can still see evidence of several other islands immersed in the chaotic region, but they are under siege by the perturbations, are very small, and with further decrease of C (increase of energy) will soon disappear.

One of the most interesting features of the satellite island structures is that they are self-similar. That is, consider any island structure. It will look similar to the overall structure, containing its own satellite island structure. Within the island structure, choose another island. It will also be a miniature copy of the larger structures, etc. The structure is infinitely complex and in a sense very well ordered. But within all this structure and order we also have regions of chaos associated with the hyperbolic points interspersed between the island elliptic points.

When $C = 3.1555$, the phase space has evolved to the structure shown in Fig. 8(c). This corresponds to orbits sampled along the line labeled C in Fig. 1(a). We see that the quasiperiodic region surrounding the elliptic point is shrinking, giving way to the encroaching chaotic region surrounding it. At this stage, a period 5 family is in the process of breaking up, and again we see evidence of other almost-destroyed islands in the chaotic region (the most prominent belong to a period 12 family, with a rotation number $\nu = 2/12$). The period 5 family causing the obvious islands is the stable counterpart of the unstable orbits represented by orbit S5 above (Fig. 5). The unstable period 5 family results from the five hyperbolic points in between the period 5 islands of Fig. 8(c).

Perhaps the most interesting feature of this figure is the trace of the first few oscillations of the stable and unstable manifolds (refer to Fig. 7). It is conjectured that orbits very close to W^u or W^s will behave similarly to the manifold they are near. Figure 8(c) lends support to this. The chaotic region results from the incredibly complex folding and refolding of W^u and W^s. In fact, the topology of W^u and W^s is a Cantor set (Guckenheimer and Holmes 1983; Wiggins 1988), and therefore fractal.

Figure 8(d) shows the phase space at $C = 3.154\,42$, corresponding to line D of Fig. 1(a). The quasiperiodic region is now dominated by a period 4 cycle. Again we can see tracers of the oscillating stable and unstable manifolds. The line $C = 3.154\,42$ happens to slice through the bifurcation struc-

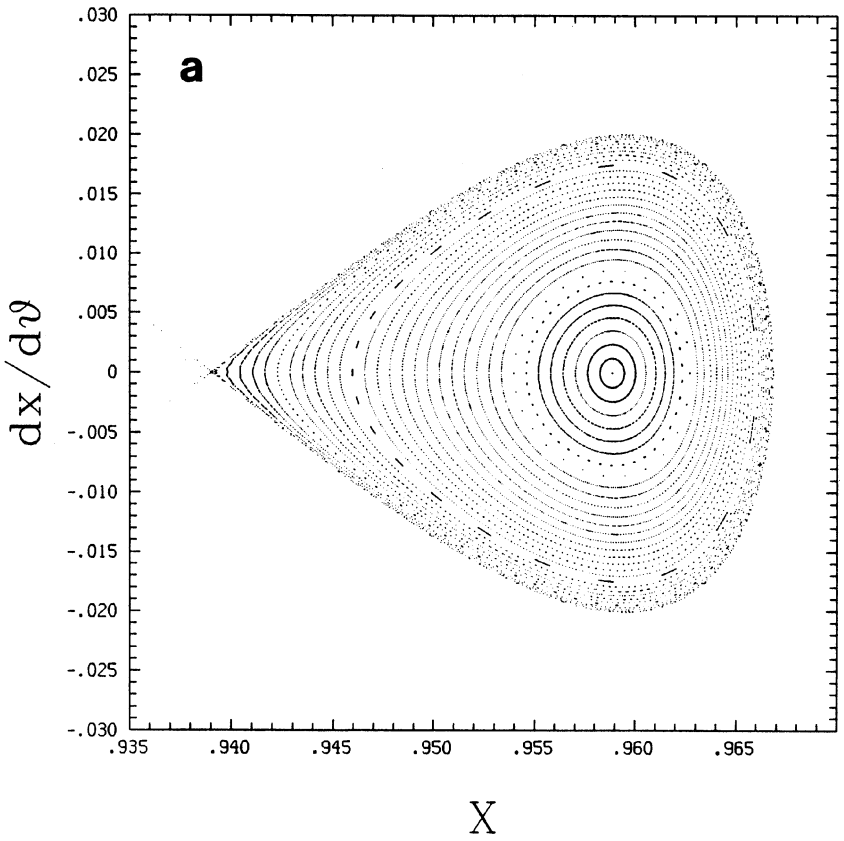

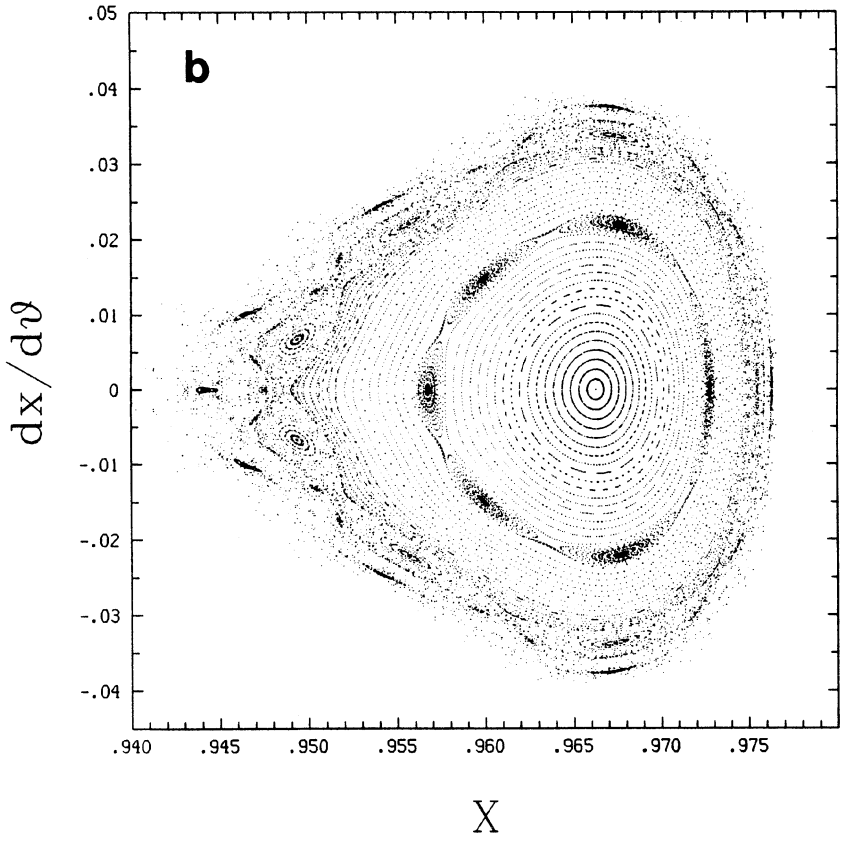

FIG. 8. Surfaces of section for (a) $C = 3.160\,36$, (b) $C = 3.157\,24$, (c) $C = 3.1555$, (d) $C = 3.154\,42$. (e) Magnification of a period 11 island immersed in the chaotic region of (d). Note the second-order satellite islands. (f) $C = 3.1536$, (g) $C = 3.152\,95$, (h) $C = 3.1525$, and (i) $C = 3.1666$. In all cases, x is the distance from the position of m_1.

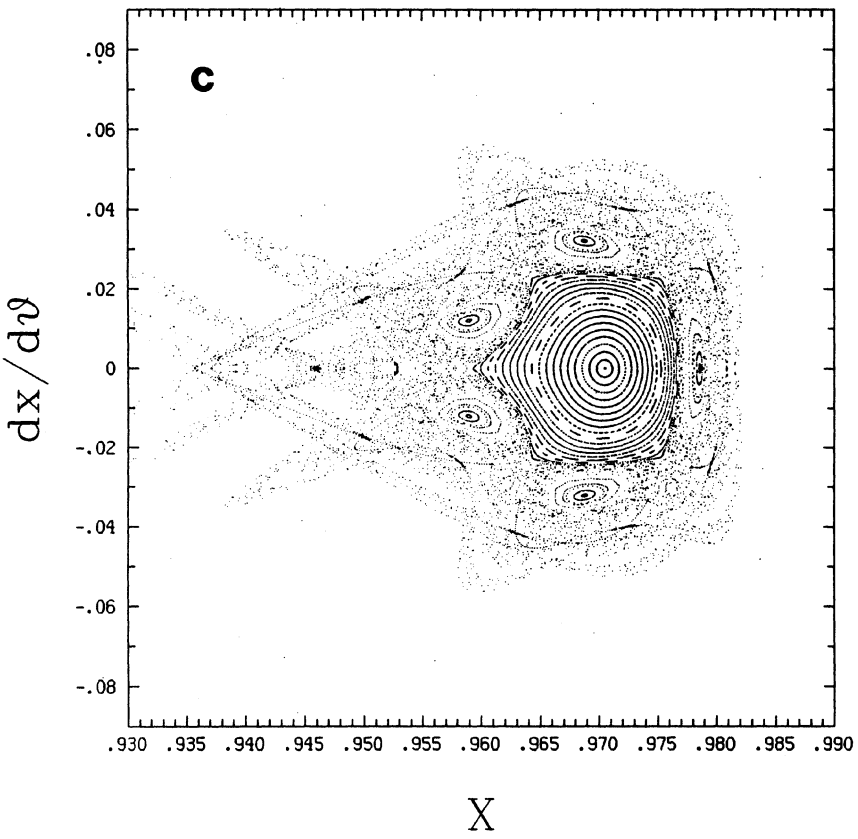

FIG. 8. (continued)

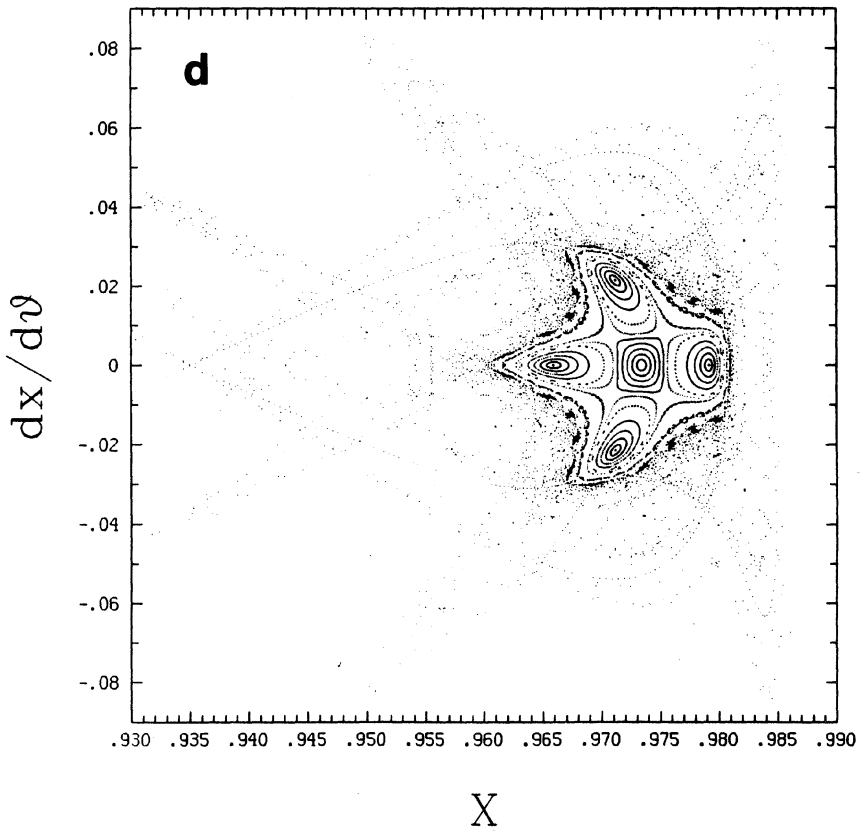

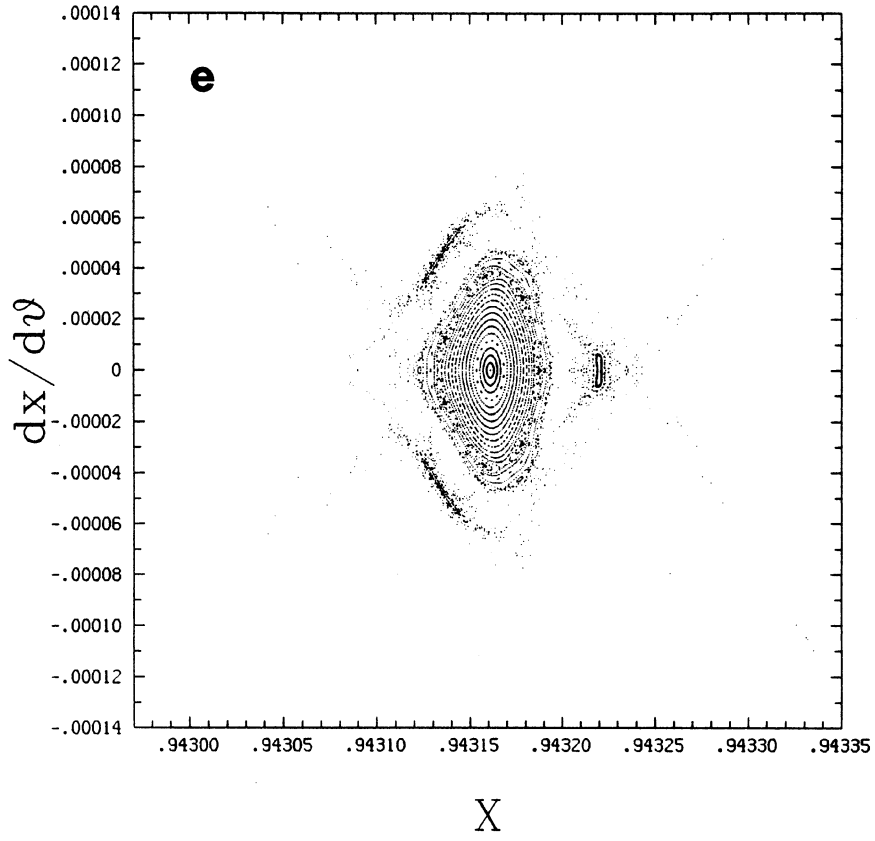

FIG. 8. (continued)

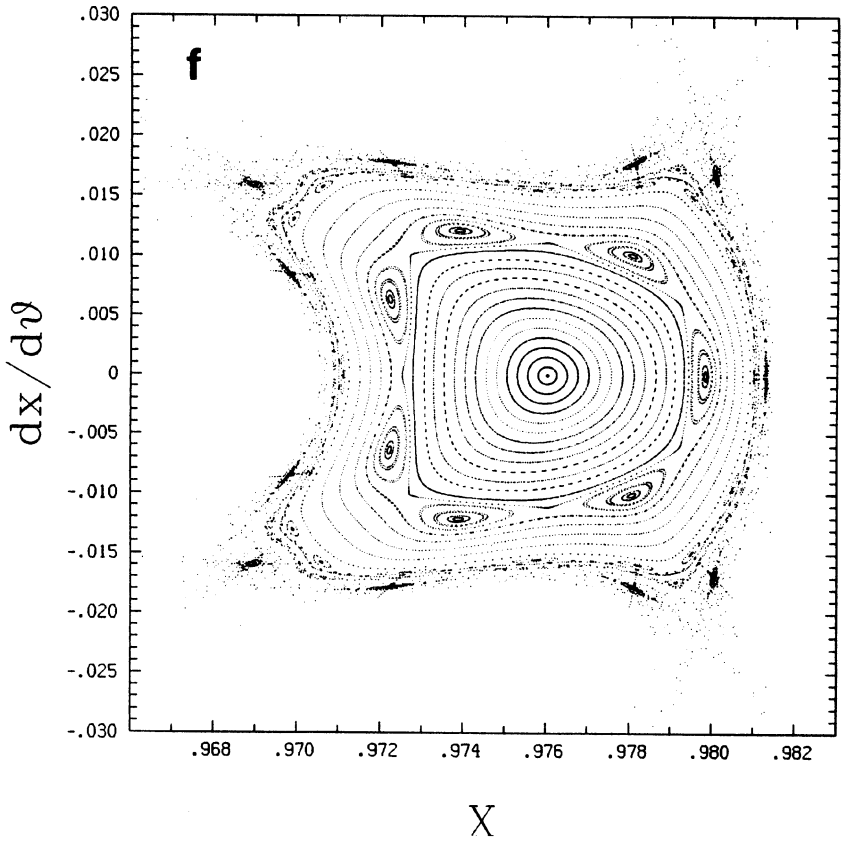

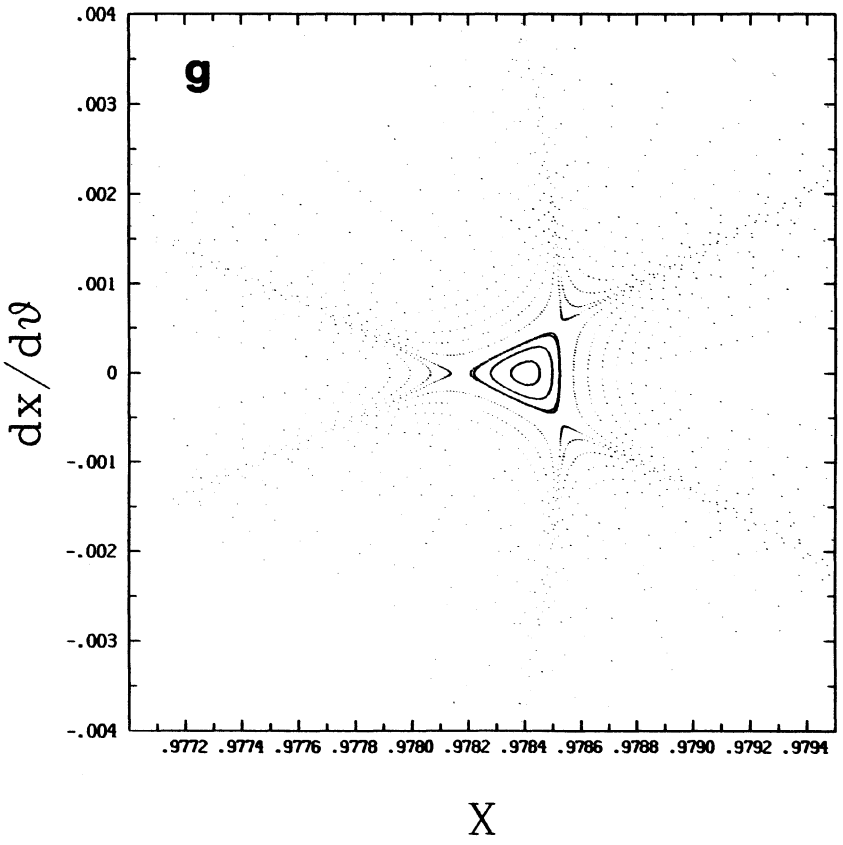

FIG. 8. (continued)

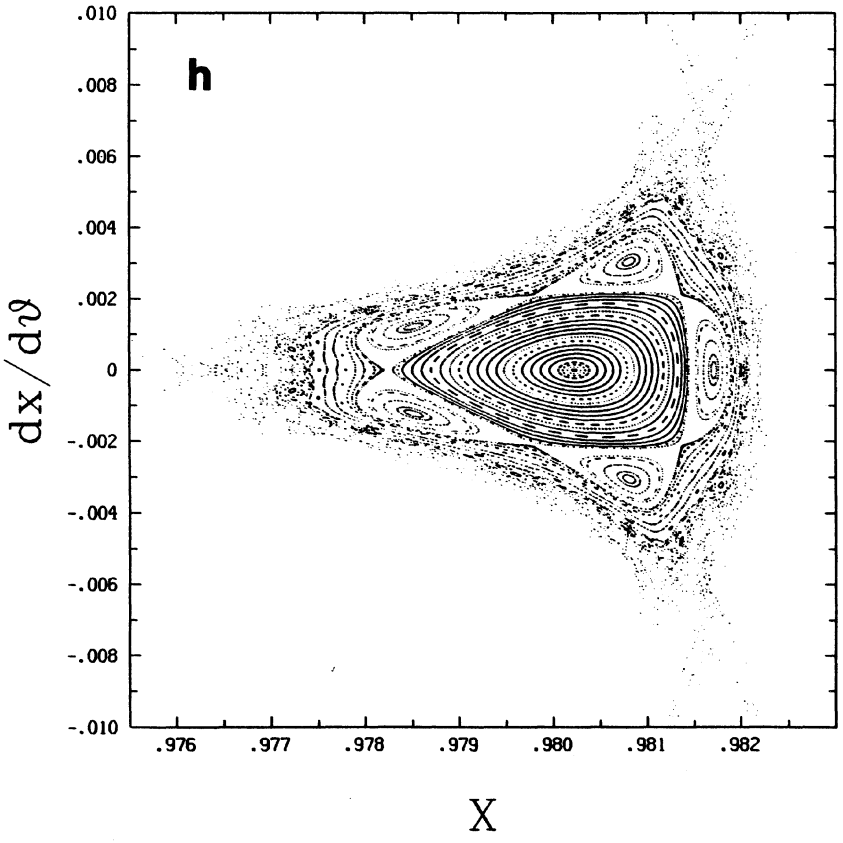

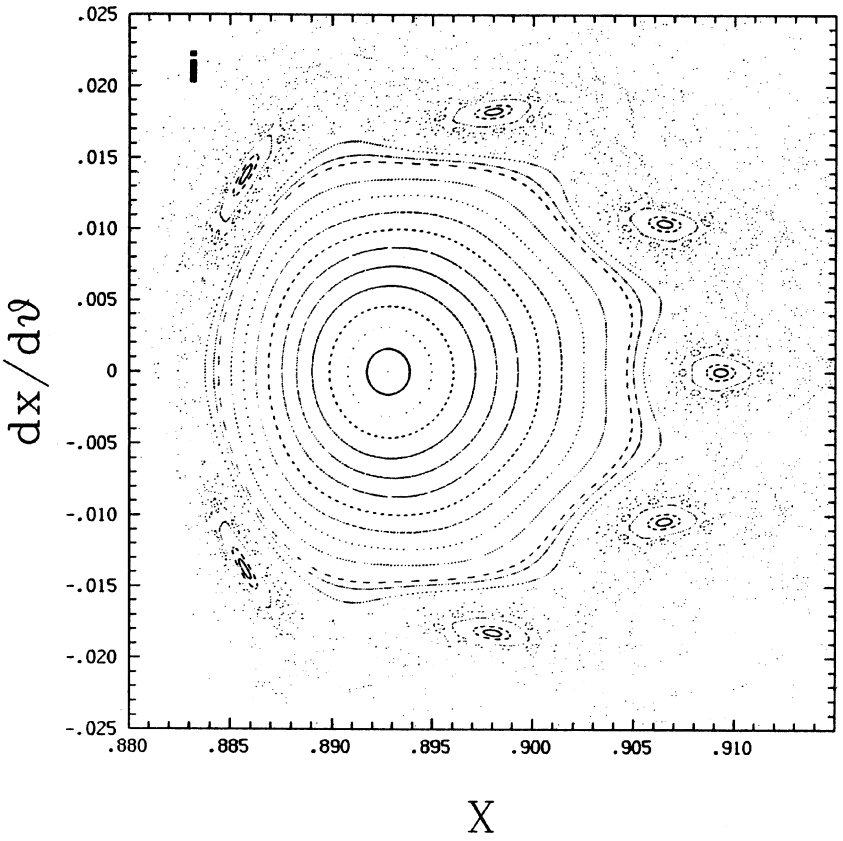

FIG. 8. (continued)

ture illustrated in Fig. 1(f). Thus, one would expect a set of 11 elliptic islands buried somewhere in the chaotic region. At the resolution of Fig. 8(d), only one orbit sampled this bifurcation area, so the islands are not readily visible on that plot. But they do exist; in fact their rotation number is $\nu = 2/11$. If one looks at a small region surrounding one of these 11 islands, one finds the structure shown in Fig. 8(e). Here we see that the period 11 elliptic point is surrounded by its own quasiperiodic region. A three-cycle surrounding this elliptic point, representing a period 33 orbit, is seen to be in the process of disappearing into the chaotic sea. One can also easily see a seven-cycle (period 77 orbit) towards the edge of the quasiperiodic zone. Thus, we see that the complicated structure apparent in the bifurcation region in Fig. 1(f) is due to the presence of elliptic islands other than just the 11 cycle alone.

Figure 8(f) shows the sos resulting from orbits sampled along line E of Fig. 1(a). Here, $C = 3.1536$. The figure illustrates only the quasiperiodic region surrounding the one-cycle and ignores most of the surrounding chaotic region. We see evidence of the breakup and disappearance of a period 4 cycle, as well as the familiar progression of elliptic island chains out through the quasiperiodic region.

The narrow neck traversed by line F of Fig. 1(a) has a phase space structure as shown in Fig. 8(g). The quasiperiodic region has shrunk drastically. Its main feature now is an unstable three-cycle. Here, the Jacobi constant is 3.152 95.

At the slightly higher energy corresponding to $C = 3.1525$ and line G of Fig. 1(a), the quasiperiodic region has expanded again as seen in Fig. 8(h). The tattered remains of the three-cycle are apparent, and the outer quasiperiodic region is dominated by a period 5 family of orbits. At still higher energy (smaller C), the quasiperiodic region shrinks again and finally is lost to the chaotic sea and disappears. This is illustrated by the disappearance of the "island" towards the bottom of Fig. 1(a).

What about the upper stability region of Fig. 1(a)? Figure 8(i) is a sos resulting from orbits sampled along the line H of Fig. 1(a) ($C = 3.1666$). We see that the phase space is again dominated by a saddle loop structure. Qualitatively similar evolution occurs with changing C as has just been discussed for the stability island. The period 1 orbit family generates a succession of n cycles as C is decreased. The quasiperiodic region shrinks and disappears into chaos below roughly 3.1642.

Orbits that escape from the influence of m_2 are, by symmetry, capture orbits. It seems from the previous analysis that a large fraction of escape orbits are chaotic. Thus, it must be that a large fraction of the orbits captured by m_2 are chaotic. To illustrate this, an orbit with initial conditions close to those of the orbit S6 above (Fig. 5) was followed after escape from m_2. The surface of section in Fig. 9 results from the ensuing motion around m_1. This single trajectory appears to fill a chaotic zone that surrounds stable quasiperiodic regions (the main quasiperiodic regions surround period 1 and period 3 cycles). This orbit is typical of the escape (and therefore capture) orbits.

The implication for the solar system is that captured satellites such as the irregular Jovian satellites originated in chaotic regions of motion about the Sun. Wisdom (1982, 1983) has shown that the 3:1 mean motion resonance with Jupiter has an associated chaotic band. This region is devoid of as-

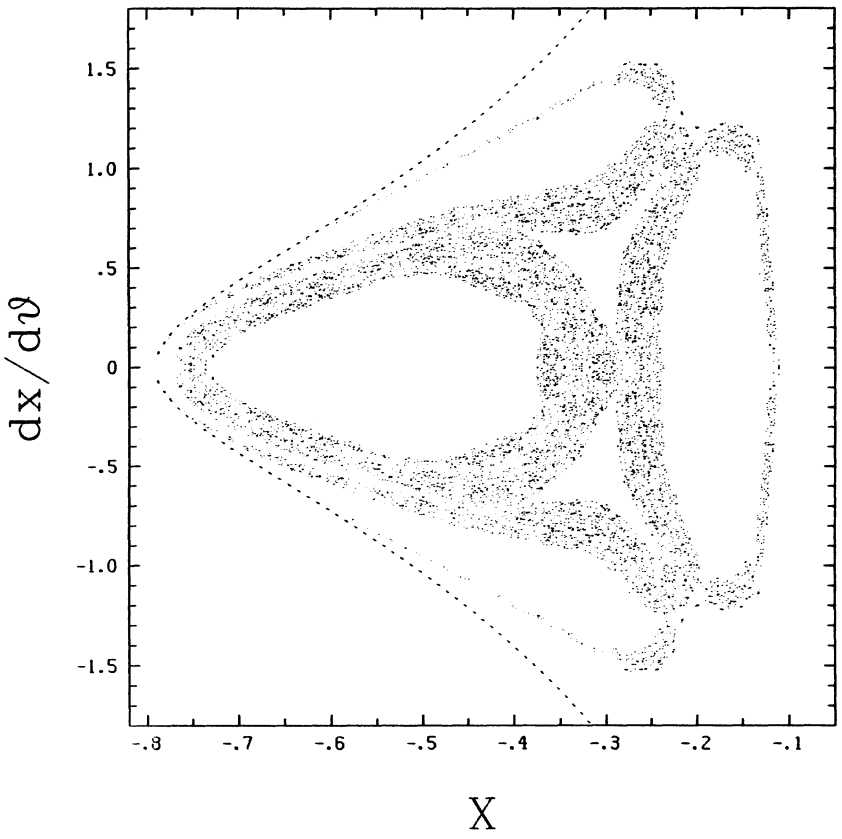

FIG. 9. Surface of section resulting from motion around m_1 after escape from m_2. All points are generated by a single trajectory. The dashed lines represent the limits of allowed motion, as determined by Eq. (1).

teroids and corresponds to one of the Kirkwood gaps. Thus he showed that chaotic motion is a mechanism for clearing a gap. Murray (1986) has done similarly for the 2:1 and 3:2 resonances. He finds a large chaotic zone at both resonances, but mentions that in the 3:2 case the chaotic zone may be overestimated. Indeed, Wisdom (1987) provides evidence that the 3:2 resonance has a very limited chaotic zone. Murison (1988, 1989b) has found that Jovian capture orbits have their origin in heliocentric orbits near the 3:2 resonance (see also Huang and Innanen 1983), which is currently occupied by the Hilda asteroids. According to Wisdom, the Hildas do not overlap the chaotic zone and appear to be stable. But the capture orbits of Murison also do not, for the most part, lie in the chaotic zone. Yet from the present work it seems that capture orbits must, in general, have a chaotic origin. This discrepancy is probably due to the fact that Wisdom has not limited his calculations to the RTBP, as have Murison and Murray.

V. CONCLUSIONS

The circular restricted three-body equations of motion have been integrated for many tens of thousands of orbits, using a fast and accurate code. The massless particle was, in each case, started in motion around the smaller primary m_2, and the amount of time before escape into motion around m_1 was determined. Because of the symmetry of the initial conditions, an escape from m_2 is the same as a capture by m_2. The capture time has been presented in the form of a gray-scale plot, with axes x_0 and C, and with gray scale proportional to capture time. A surprising complexity results, with the various loops and strands corresponding to families of periodic orbits.

We have found that the structures of periodic orbit families in the C–x_0 initial conditions plane are infinitely complex, self-similar, and probably fractal. A sequence of successive magnifications in the C–x_0 plane illustrates the point. As in many other nonlinear dynamical systems, such structure appears at the boundary of attracting regions. In this case, the "attractors" consist of the tendency of the massless particle to orbit either m_1 or m_2. The boundary itself is infinitely complex. Thus, satellite capture is a boundary effect, and the boundary is infinitely complex. We have also shown illustrative cases of period-doubling and nonperiod-doubling bifurcations of periodic orbit families.

A surface of section analysis of selected regions of the C–x_0 plane greatly illuminates the features of the C–x_0 structures. We reaffirm that the loops and strands are tracers of periodic orbit families. The finite capture time areas correspond to motion in the chaotic regions of the sos plots, while the infinite capture time areas are regions where the motion is trapped in the quasiperiodic islands surrounding elliptical fixed points. The complex C–x_0 structure is a result of the complex phase space structure as illustrated in the surfaces of section. The changes in this complex, fractal-like structure with changing energy are explained by the evolution of the various elliptic and hyperbolic n cycles and their associated quasiperiodic and chaotic regions. Structures appear and disappear as bifurcations give birth to new cycles and as the chaotic sea swallows them up. The main stability feature, or "island," of the C–x_0 plane is the result of the birth, at the top, of a saddle-loop structure and the corresponding quasiperiodic region surrounding the stable fixed point. As the

energy is increased, perturbations cause a transversal intersection of the stable and unstable invariant manifolds of the hyperbolic-fixed point, leading to wild oscillations of the invariant manifolds, a homoclinic tangle, and chaotic dynamics. Qualitatively similar phenomena are also occurring for the upper stability region of Fig. 1(a).

One of the interesting features found on the surface of section plots is due to orbits lying close to the stable and unstable invariant manifolds. At the resolution of the figures, the first few oscillations of the manifolds are easily seen.

With regard to gravitational satellite capture in the solar system, an implication of this work is that an important mechanism of capture is capture of chaotic orbits. Most, if not all, escape (= capture by symmetry) orbits appear to be chaotic. Thus, we propose that captured satellites originated from chaotic orbits around the Sun. This is currently being explored further, for actual solar system mass ratios. [Murison (1988, 1989b) has shown that the mass ratio μ has a major effect on the structure of phase space.]

Integration of the full differential equations of motion of a dynamical system such as even the RTBP is very time consuming. Surface of section explorations can be accomplished much more quickly with iterative mappings. Wisdom (Wisdom 1982, 1983; Tittemore and Wisdom 1988, 1989) has managed to construct iterative maps of the RTBP that are valid near certain mean motion resonances in the solar system. The capture time diagrams of this paper (Figs. 1), and the phase space behavior evident in the sos plots, bear a striking resemblance to those corresponding to an iterative map investigated by MacKay (1984). Vazquez *et al.* (1987) have found similarities between the dynamics of the Cremona iterative map and the RTBP. These examples provide hope that an iterative map can perhaps someday be found that will have qualitatively the same dynamics as the RTBP.

The author would like to thank Arthur D. Code, Marc Balcells, and Barbara A. Whitney for support, useful discussions, and encouragement at crucial times. Computing was performed at the Midwestern Analysis and Data Reduction Facility (MADRAF); generous allocation of resources is acknowledged and greatly appreciated. He also thanks the referee for useful comments.

REFERENCES

Bettis, D. G., and Szebehely, V. (1971). Astrophys. Space Sci. **14**, 133.
Euler, L. (1772). *Theoria Motuum Lunae* (Typis Academiae Imperialis Scientiarum, Petropoli).
Feder, J. (1988). *Fractals* (Plenum, New York).
Guckenheimer, J., and Holmes, P. (1983). *Nonlinear Oscillations, Dynamical Systems, and Bifurcations of Vector Fields* (Springer, New York).
Helleman, R. (1984). In *Universality in Chaos*, edited by P. Cvitanovic (Hilger, Bristol), p. 420. Also in *Fundamental Problems in Statistical Mechanics* (1980) edited by E.G.D. Cohen (North-Holland, Amsterdam), Vol. 5, p. 165.
Hénon, M. (1965a). Ann. Astron. **28**, 499.
Hénon, M. (1965b). Ann. Astron. **28**, 992.
Hénon, M. (1969a). Bull. Astron. **3**, 57.
Hénon, M. (1969b). Bull. Astron. **3**, 49.
Hénon, M. (1969c). Astron. Astrophys. **1**, 223.
Hénon, M. (1983). In *Chaotic Behaviour of Deterministic Systems*, edited by G. Iooss, R. Helleman, and R. Stora (North-Holland, Amsterdam).
Huang, T.-Y., and Innanen, K.A. (1983). Astron. J. **88**, 1537.
Jefferys, W. H. (1974). Astron. J. **79**, 710.
MacKay, R. S. (1984). In *Universality in Chaos*, edited by P. Cvitanovic (Hilger, Bristol), p. 412.
Mandelbrot, B. B. (1982). *The Fractal Geometry of Nature* (Freeman, New York).
Mandelbrot, B. B. (1986). In *Fractals in Physics*, edited by L. Pietronero and E. Tosatti (North-Holland, Amsterdam).
McDonald, S. W., Grebogi, C., Ott, E., and Yorke, J. A. (1985). Physica **17D**, 125.
Murison, M. A. (1988). Ph.D. thesis, University of Wisconsin–Madison.
Murison, M. A. (1989a). Astron. J. **97**, 1496.
Murison, M. A. (1989b). In preparation.
Murray, C. D. (1986). Icarus **65**, 70.
Nacozy, P. E. (1971). Astrophys. Space Sci. **14**, 40.
Peitgen, H.-O., and Richter, P. H. (1986). *The Beauty of Fractals* (Springer, New York).
Poincaré H. (1892, 1893, 1899). *Les Methodes Nouvelles de la Mecanique Celeste* (Gauthier–Villars, Paris), Vols. 1–3.
Press, W. H., Flannery, B. P., Teukolsky, S. A., and Vetterling, W. T. (1986). *Numerical Recipes: The Art of Scientific Computing* (Cambridge University, Cambridge).
Roy, A. E., and Ovenden, M. W. (1955). Mon. Not. R. Astron. Soc. **115**, 297.
Ruelle, D. (1989). *Elements of Differentiable Dynamics and Bifurcation Theory* (Academic, Boston).
Stiefel, E., and Scheifele, G. (1970). *Linear and Regular Celestial Mechanics* (Springer, New York).
Szebehely, V. (1967). *Theory of Orbits* (Academic, New York).
Tittemore, W. C., and Wisdom, J. (1988). Icarus **74**, 172.
Tittemore, W. C., and Wisdom, J. (1989). Icarus **78**, 63.
Vazquez, E. C., Jefferys, W. H., and Sivaramakrishnan, A. (1987). Physica **29D**, 84.
Wiggins, S. (1988). *Global Bifurcations and Chaos* (Springer, New York).
Wisdom, J. (1982). Astron. J. **87**, 577.
Wisdom, J. (1983). Icarus **56**, 51.
Wisdom, J. (1987). Icarus **72**, 241.

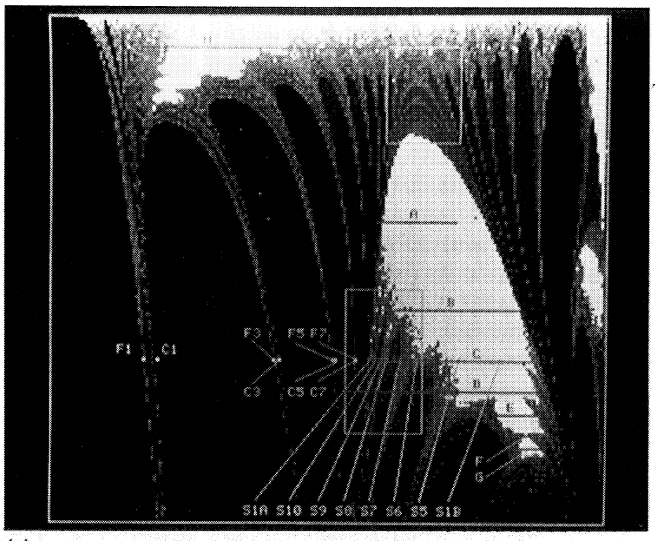

(a)

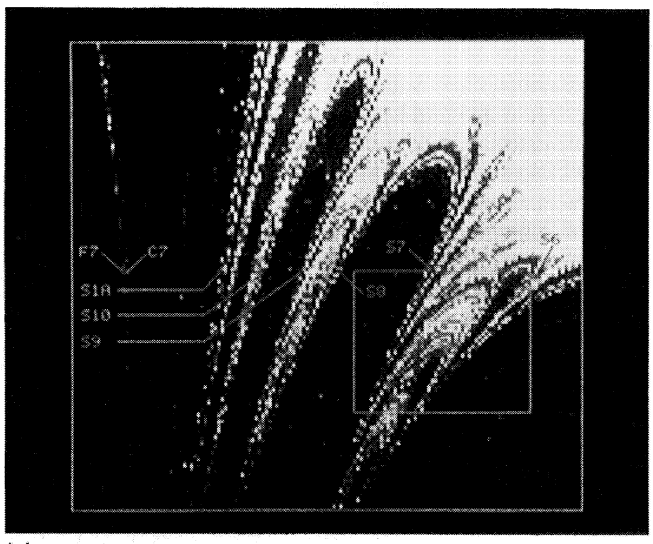

(b)

FIG. 1. (a) C–x_0 CRTB diagram for $\mu = 0.01$. Horizontal axis is initial position x_0, and vertical axis is Jacobi constant C. (b) Magnification of the lower box of (a). (c) Magnification of the boxed region of (b). (d) Magnification of the boxed region in (c). (e) Magnification of the lower box of (d). (f) Magnification of the upper boxed region of (d). (g) Magnification of the upper box of (a). (h) Magnification of the boxed region of (g).

Marc A. Murison (see page 2347)

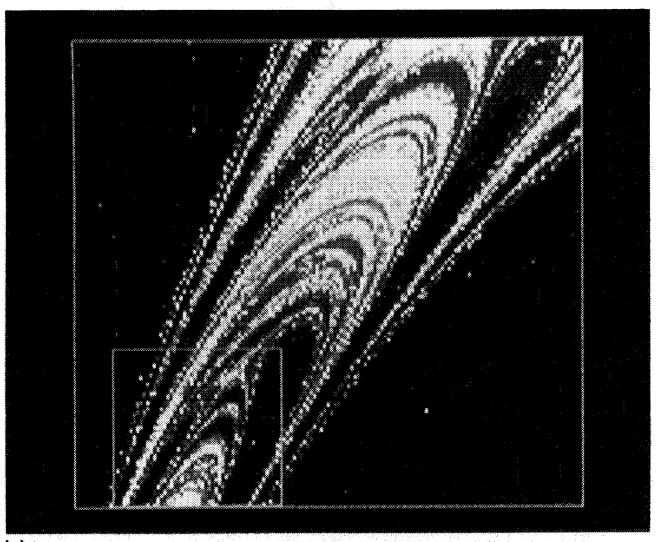

(c)

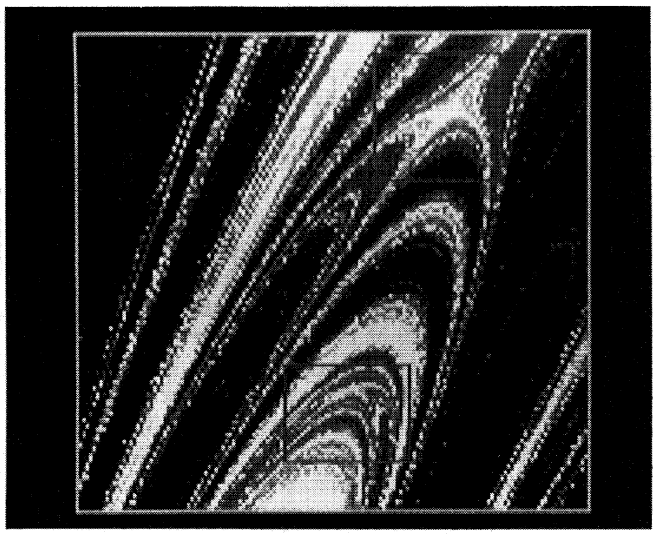

(d)

FIG. 1. (continued)

Marc A. Murison (see page 2347)

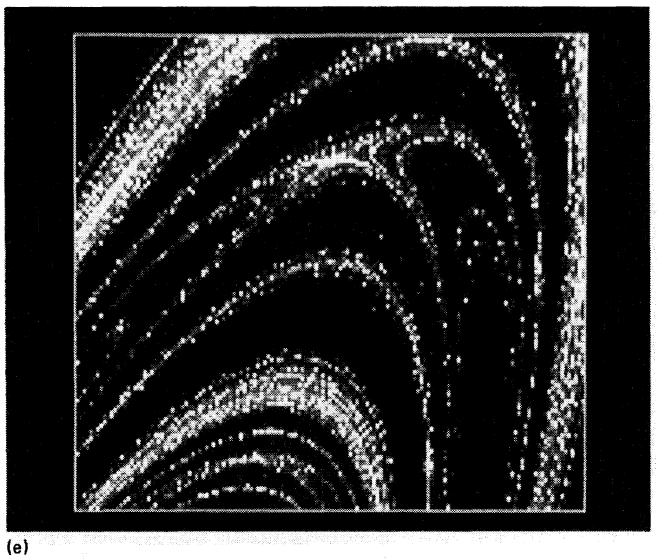

(e)

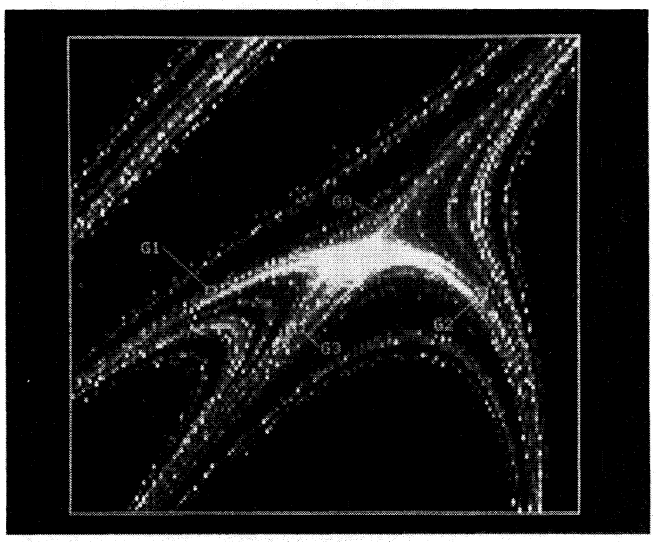

(f)

FIG. 1. (continued)

Marc A. Murison (see page 2347)

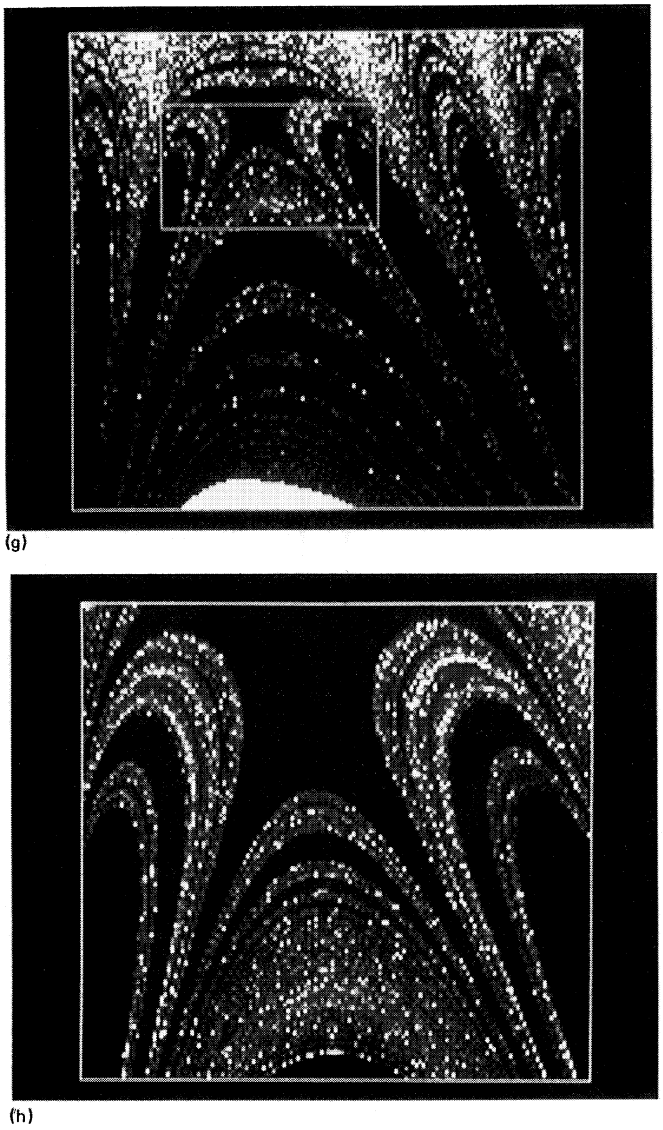

FIG. 1. (continued)

Marc A. Murison (see page 2347)